Ceramics International 44 (2018) 2539–2546

Contents lists available at ScienceDirect

Ceramics International

journal homepage: www.elsevier.com/locate/ceramint

High temperature properties of $Sr_2MgMo_{0.9}TM_{0.1}O_{6-\delta}$ (TM = Mn, Co and Ni)

P.K. Dager[a], L.V. Mogni[a,b,*], S. Soria[a,b], A. Caneiro[a,b]

[a] Centro Atómico Bariloche (CAB) – Comisión Nacional de Energía Atómica (CNEA), Av. Bustillo 9500 S.C. de Bariloche, CP 8400, Argentina
[b] Consejo Nacional de Investigaciones Científicas y Técnicas (CONICET), Av. Rivadavia 1917 (C1033AAJ), Buenos Aires, Argentina

ARTICLE INFO

Keywords:
C) Electrical conductivity
C) Thermodynamic stability
D) $Sr_2MgMoO_{6-\delta}$ double perovskite
E) SOFC electrode

ABSTRACT

High temperature properties of $Sr_2MgMo_{0.9}TM_{0.1}O_{6-\delta}$ (SMMTM; TM = Mn, Co and Ni) and $Sr_2MgMo_2O_6$ (SMMO) compounds were studied for evaluating SMMTM materials as SOFC electrodes. SMMTM and SMMO compounds were synthesised by the combustion method, followed by annealing in air at temperatures between 1000 and 1200 °C. Rietveld structural analysis of XRD patterns showed that the TM-dopants substitute Mo cations with a solubility limit of 10% of Mo. SMMTM compounds are thermodynamically stable in 10%H_2-Ar until 900 °C. Electrical conductivities of SMMTM under reducing atmosphere were three orders of magnitude higher than in air. Although the partial replacement of Mo by Mn or Ni in $Sr_2MgMoO_{6-\delta}$ decreases the electrical conductivity in both atmospheres, an increase of conductivity in 10%H_2 atmosphere was observed for SMMCo compound. Whilst the area specific resistance (ASR) are not significantly affected by Mo-substitution in reducing atmospheres, the ASR of SMMTM materials as cathodes are improved.

1. Introduction

Solid Oxide Fuel Cells (SOFCs) are electrochemical devices that directly convert chemical energy into electrical energy with high efficiency, little pollutant emissions and fuel flexibility [1–3]. Although Ni-based anodes were initially the most used for SOFCs, they exhibited some drawbacks such as their reactivity with $La_{0.8}Sr_{0.2}Ga_{0.83}Mg_{0.17}O_{2.815}$ (LSGM) electrolyte, low stability towards fuel impurities (sulphur), and carbon deposition (coking) when hydrocarbons are used as fuels. Also, the volume changes associated with Ni to NiO during oxidation/reduction cycles produce mechanical stresses [2–4].

Many efforts have been made to develop oxides with mixed ionic-electronic conductivity (MIECs) as anode materials since they could be less susceptible to coking and sulphur poisoning [2,3,5–7]. Perovskite materials based on strontium titanantes ($La_{0.4}Sr_{0.6}Ti_{1-x}Mn_xO_{3-x}$) [8] and lanthanum chromites ($La_{1-x}Sr_x)_{0.9}Cr_{0.5}Mn_{0.5}O_{3-x}$ (LSCM) [9] are emerging as attractive candidates for SOFC's anodes. LSCM perovskite is a mixed ionic electronic conductor (MIEC) which has shown good catalytic activity for humidified-H_2 and CH_4 based fuels, but its electronic conductivity is low and the stability in sulphur-containing fuel is poor [5,10,11].

Huang et al. reported that the $Sr_2MgMoO_{6-\delta}$ (SMMO) double-perovskite, which contains alternating MgO_6 and MoO_6 corner-shared octahedra [12], is a MIEC showing high power density when methane is used as fuel [3,6]. This material is stable in reducing atmosphere at temperatures higher than 1000 °C and it shows a good tolerance to sulphur poisoning [4,13–15]. Nevertheless, the electrical conductivity values reported for this material are lower than those of Ni-YSZ anodes [11,16]. Because of this, new alternatives for improving the electrical properties of Sr_2MgMoO_6 compound should be explored.

Substitutions on A(Sr) and/or B sites (Mg and Mo) with alkali earth (or rare earth-metal) and transition metal elements, respectively, offer the possibility to improve the electrical conductivity, electrocatalytic activity and chemical stability of SMMO. Doping Sr-site with La provides a better performance of the anode in the SOFCs [17] but it was also observed that this compound presents segregation of secondary phases; $SrMoO_4$ and La_2O_3 under oxidising atmospheres. The above mentioned is a disadvantage for practical applications because the fabrication process for SOFC is performed in air [18]. Most of the studies were focused on the effect of substitution on Mg-site by 3d-transition metals; hence, the electrical conductivity of SMMO is enhanced by Al or Co substitution on Mg-site [19,20]. Similarly, the electrochemical performance of SMMO as anode is improved by Al and Co doping. Nonetheless, it has been reported that electrical conductivity depends on the temperature of synthesis and reducing conditions [13,19,21].

The substitution at Mo-site was also evaluated by doping it with

* Corresponding author at: Centro Atómico Bariloche (CAB) – Comisión Nacional de Energía Atómica (CNEA), Av. Bustillo 9500 S.C. de Bariloche, CP 8400, Argentina.
E-mail addresses: mogni@cab.cnea.gov.ar, lilianamogni@gmail.com (L.V. Mogni).

http://dx.doi.org/10.1016/j.ceramint.2017.11.006
Received 7 October 2017; Received in revised form 31 October 2017; Accepted 1 November 2017
Available online 07 November 2017

transition metals with high oxidation state, such as W, Nb [6] or V [22]. Although it has been reported that doping with Nb on Mo-site for SMMO double perovskite is useful to enhance its SOFC anode performance, there are also adverse effects such as the reduction of the electrical conductivity for $Sr_2MgMo_{0.8}Nb_{0.2}O_{6-\delta}$ (SMMNb) compound under reducing conditions [6]. Furthermore, electrochemical measurements for SMMNb under methane atmosphere indicate that the adsorption of carbonaceous species limits the fuel oxidation process increasing the area specific resistance and reducing the power density [23].

In the present work, a new approach is tested: partial substitution of Mo by 3d-transition metals. $Sr_2MgMo_{0.9}A_{0.1}O_{6-\delta}$ samples (SMMTM; TM = Mn, Co, and Ni) were synthesised in order to explore their potential use as an alternative SOFC-anode material. In this context, relevant electrodes high temperature properties of SMMTM were systematically evaluated. The effects of each transition metal (Mn, Co, or Ni) on crystal structure, thermodynamic stability, electrical conductivity and area specific resistance of $Sr_2MgMoO_{6-\delta}$ compound were analysed. Finally, the electrochemical performance under oxidising atmosphere was studied to evaluate the use of these compounds in symmetrical cell configuration (S-SOFC).

2. Experimental procedure

$Sr_2MgMo_{0.9}TM_{0.1}O_{6-\delta}$ (SMMTM; TM = Mn, Co, Ni) and $Sr_2MgMoO_{6-\delta}$ (SMMO) materials were synthesised by the combustion-solution method [24–26]. Stoichiometric amounts of $SrCO_3$ and Mg were dissolved in a diluted HNO_3 solution, whilst MoO_3 was dissolved in NH_4OH solution. In order to dope with Mn or Co, metallic-manganese and cobalt powder were separately dissolved in a diluted HNO_3 solution. On the other hand, SMMNi was prepared similarly to SMMCo and SMMMn, but by using a $Ni(NO_3)_26H_2O$-solution instead of metallic Ni. Glycine in a stoichiometric amount of combustible to metal ions of $\varphi = 2.8$ and 50% w/w of NH_4NO_3 were added to the nitrate solution followed by a soft heating at ~ 200 °C until auto-ignition was reached [26]. The ash-precursors were thermally treated in air at the optimised conditions of 1000 °C-12 h for SMMO and SMMMn, 1200 °C-10 h for SMMCo and 1100 °C-12 h for SMMNi.

X-Ray diffraction (XRD) measurements were performed to evaluate the crystal structure, as well as structural stability after thermogravimetry studies and during the storage time of the SMMO and SMMTM powders. The chemical compatibility between anode materials (SMMO and SMMTM powders) and electrolytes (LSGM and GDC) was also assessed by using this technique. XRD data were collected by using a Panalytical Empyrean diffractometer equipment with Cu-Kα radiation ($\lambda = 0.1542$ nm) and 3D PIXcel detector within $10^\circ \leq 2\theta \leq 110^\circ$ range. Rietveld refinements of the XRD patterns were performed by using FULLPROF tools [27]. The morphology and chemical composition of the samples were examined by scanning (SEM) and transmission (TEM) electron microscopy using a SEM-FEG FEI NovaNano SEM 230 and a Philips CM 200 UT (LaB_6) microscope, respectively. Both microscopes are equipped with an Energy Dispersive Spectrometer (EDS).

Thermogravimetric analyses (TGA) were carried out in order to determine the thermodynamic stability under reducing (10%H_2-Ar gas flow) and oxidising (air) atmospheres. The TGA were performed by using a highly sensitive thermogravimetric equipment consisting of a symmetrical thermobalance based on a Cahn 1000 electrobalance [28]. The thermobalance allows the determination of sample mass changes within ± 10 μg at high temperatures for about 0.25 g powder samples of SMMTM.

The electrical conductivity of all samples was measured by conventional four probe DC method by using an Agilent 3497A scanner-multimeter. Dense samples were obtained by uniaxial pressing of SMMTM powders followed by a thermal treatment in air at 1300 °C during 4 h. Pt wire and Ag paste were used to make the electrical contacts. The equilibrium conductivity measurements were carried out at temperatures between 600 and 800 °C with an interval of 50 °C. The measurements were performed in air by increasing temperature and waiting until sample resistance reached a constant value. Once at 800 °C, the atmosphere was switched to 10%H_2-Ar and, after annealing for 10–12 h, the electrical conductivity under reducing atmosphere was measured decreasing temperature.

Prior to Electrochemical Impedance Spectroscopy (EIS) measurements, the chemical compatibility between the electrode and two electrolytes was evaluated. Sr_2MgMoO_6 powders were mixed with $La_{0.8}Sr_{0.2}Ga_{0.83}Mg_{0.17}O_{2.815}$ (LSGM) and $Ce_{0.95}Gd_{0.10}O_{1.95}$ (GDC) electrolytes in the weight ratio 1:1, respectively. The mixed powders were thermally treated in air for 6 h between 800 and 1200 °C. The possibility of reactivity with formation of new phases was checked by XRD after the thermal treatments.

EIS measurements were performed on a symmetrical SMMTM/GDC/SMMTM cells configuration. Dense GDC electrolytes of 600 μm thickness were prepared by sintering the pellets in air at 1350 °C during 4 h. SMMO or SMMTM symmetrical electrodes were coated onto these dense GDC pellets using a slurry prepared by mixing SMMO or SMMTM powders with PVB, PVP and α-terpineol diluted in isopropyl alcohol. This slurry was deposited onto both surfaces of the electrolyte by spin coating and then annealing in air at 1000 °C for 3 h. The EIS spectra were collected, using Pt-grids as current collectors, between 500 and 800 °C under 10%H_2 – Ar and dry air. The low electrical conductivity under oxidising conditions required the use of porous $La_{0.85}Sr_{0.15}MnO_3$ (LSM) layer as current collector, deposited on ~25 μm thick SMMO and SMMTM electrodes. The EIS measurements were performed in a frequency range 10^6–10^{-3} Hz with signal amplitude of 50 mV at 0 V bias voltage by using a frequency response analyser (FRA) coupled to an AUTOLAB PGSTAT30 potentiostat.

3. Results and discussion

As stated above, most of studies about Sr_2MgMoO_6 compound were focused on the partial substitution of Mg^{2+} by other divalent transition metal ions. In contrast with those researches, the aim of the present work was to explore the effect of partial substitution of Mo by transition metals with lower oxidation states. The existence of cationic defects in which the Mg(Mo) occupies Mo(Mg) position or anti-site defect could be present in this kind of perovskite [14], a structural study by Rietveld method allows to analyse this as well as the change of symmetry and sample purity.

Figs. 1a–c present the XRD patterns and Rietveld refinement for the as-synthesised SMMMn, SMMCo and SMMNi compounds, respectively. The formation of the double perovskite phase was achieved for all compounds with small amounts of SrO, $SrCO_3$ and MgO impurities (see Fig. 1d, total impurities < 4%w/w). It should be noted that $Sr_2Mg_{1-x}Co_xMoO_{6-\delta}$ and $Sr_2Mg_{1-x}Ni_xMoO_{6-\delta}$ compounds, synthesised by other authors [20,29] tolerate substitutions up to $x = 0.7$ and $x = 0.9$ respectively on Mg-site with no evidence of impurities. However, the partial substitution of Mo by Mn, Co or Ni in $Sr_2MgMo_{1-x}TM_xO_{6-\delta}$ with $x > 0.1$ caused significant amount of impurities. Therefore, the solubility limit of Mn, Co and Ni on Mo-site of SMMO double perovskite is $x \sim 0.10$. Despite the low solubility limit, the substitution of Mo, with valence +5/+6, by other di- and trivalent transition metal allowed to increase the concentration of oxygen vacancies, contrary to those observed when Mg^{2+} was partially substituted with the same cations. On other hand, by using this synthesis method and compositions, the non-doped and doped double perovskites were obtained under air atmosphere, lower temperature and shorter times in comparison with literature data which report synthesis temperatures higher than 1200 °C, annealing times above 20 h and reducing atmosphere [7,12,14,15,23]. Regarding the structural stability of the samples during the storage time, diffraction peaks related to $SrMoO_4$ impurity were detectable on the XRD patterns for SMMTM samples stored in air during long periods of time (> two months). Nevertheless, a thermal treatment in air at

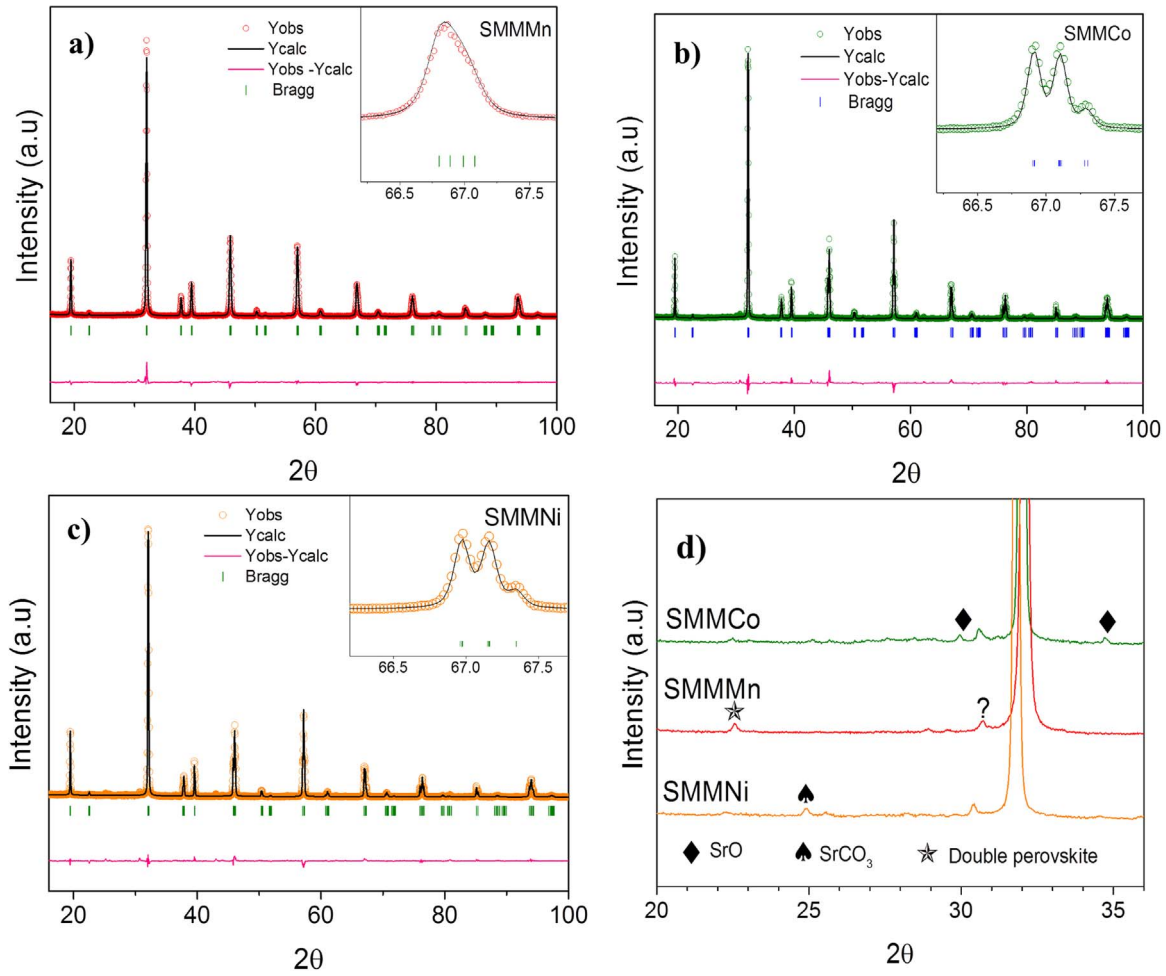

Fig. 1. XRD patterns and their Rietveld refinement profiles of **a)** $Sr_2MgMo_{0.9}Mn_{0.1}O_{6-\delta}$ (SMMMn) **b)** $Sr_2MgMo_{0.9}Co_{0.1}O_{6-\delta}$ (SMMCo) and **c)** $Sr_2MgMo_{0.9}Ni_{0.1}O_{6-\delta}$ (SMMNi). Insets: magnification of XRD patterns between 66.0 and 67.8° which is indicative of structural difference among samples **d)** High magnification of XRD patterns between 20 and 36° indicating the presence of impurity peaks.

900 °C for 2 h was enough for $Sr_2MgMo_{0.9}TM_{0.1}O_{6-\delta}$ compounds to recover the original $SrMoO_4$-free sample

Table 1 summarises the structural parameters of the SMMTM powders determined by Rietveld refinement of the XRD data. For SMMCo and SMMNi samples the refinements were performed by using a structural model previously reported by Bernuy-Lopez et al. [14] based on the assumption of a triclinic $I\bar{1}$ space group. Otherwise, a tetragonal structure $I4/m$ reported by Sher et al. [30] was used for SMMMn. The insets in each SMMTM-diffraction patterns of Fig. 1a–c show the different shapes of peaks at about 67°. This peak is one of the most sensitive to the change of symmetry. This structural variation (from triclinic to tetragonal structure) was also observed for Sr_2MgMoO_6 samples doped with Fe on Mg site [12].

The structural models used in this work explore the possibility of anti-site defect of Mo(TM) and Mg cations between both, Mo and Mg sites (see Table 1). The results of this study confirm the preference of TM-cations (TM = Mn, Co, Ni) to be located on Mo-site under the synthesis conditions tested in this work. The structural analysis also indicates that the lattice is compressed in the *c* direction and expanded in the *a-b* plane as a consequence of partial substitution of Mo by Mn, Co or Ni, with a net reduction of the unit cell volume, mainly for TM = Co or Ni. Moreover, the anti-site defect values decrease for the samples doped with Co and Ni.

Fig. 2 shows SEM and TEM micrographs for the SMMTM samples. SMMMn sample shows highly interconnected grains with relatively homogenous size and porous morphology, whilst SMMCo and SMMNi powders, synthesised at higher temperatures show a higher degree of densification. The increment of grain size from 200 to 350 nm for SMMMn, SMMNi and approximate 1 μm for SMMCo is attributed to a

Table 1
Structural parameters of SMMTM (TM = Mn, Co, and Ni) samples synthesised in air at 1000 °C, SMMMn; 1200 °C, SMMCo; 1100 °C, SMMNi. * Lattice parameters for SMMO compound thermally treated at 1000 °C during 12 h are $a = 5.5762$ Å, $b = 5.5753$ Å, $c = 7.9258$ Å, $V = 246.40$ Å^3, $\alpha = 89.995$, $\beta = 89.984$ and $\gamma = 89.997$ [26].

SMMTM (TM = Mn, Co, Ni) Parameters*	SMMMn TT 1000°C_12 h	SMMCo TT 1200°C_10 h	SMMNi TT 1100 °C 12 h
a (Å)	5.59070(1)	5.5889(8)	5.5846(7)
b (Å)	5.59070(1)	5.5892(7)	5.5854(7)
c (Å)	7.9247(4)	7.8842(8)	7.8774(7)
α (°)	90.000	90.018(10)	89.997(11)
β (°)	90.000	89.997(10)	90.000
γ (°)	90.000	89.704(6)	89.726(5)
V (Å^3)	247.694(15)	246.28(5)	245.71(5)
F_{Occ}(%)			
Mg-site	2*a* (0,0,0)	2*a* (0,0,0)	2*a* (0,0,0)
Mg/Mo/TM	98.0/1.8/0.2	90.4/8.6/1.0	91.6/7.6/0.8
Mo-site	2*b* (0,0,1/2)	2*e* (1/2, 1/2, 0)	2*e* (1/2, 1/2, 0)
Mg/Mo/TM	2.0/88.2/9.8	9.6/81.4/9.0	8.4/82.4/9.2
R_p	10.2	14.0	11.9
R_{wp}	11.5	15.1	13.6
χ^2	3.2	3.6	3.0
Impurities (%)	–	< 3	< 4

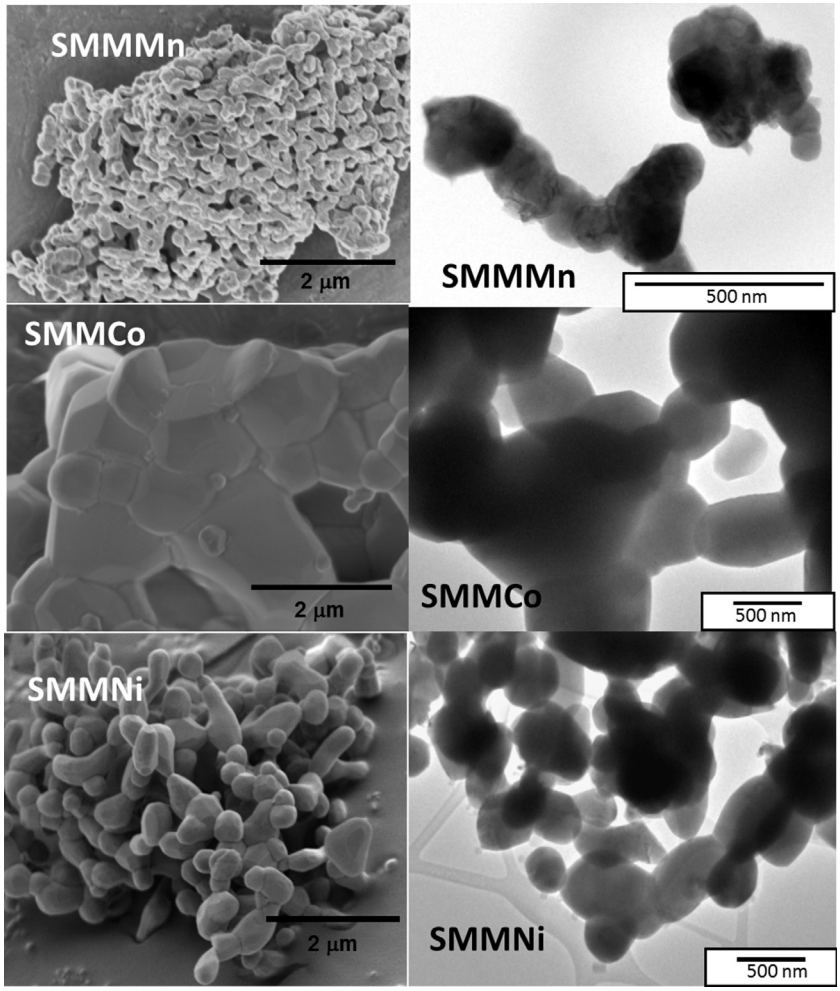

Fig. 2. SEM (left column) and TEM bright field (right column) micrographs of SMMTM samples synthesised in air at 1000 °C-12 h for SMMMn, 1200 °C-10 h for SMMCo, and 1100 °C-12 h for SMMNi.

rising of synthesis temperatures from 1000 to 1100–1200 °C, respectively.

Fig. 3 shows the mass evolution with time for SMMO and SMMTM compounds in dry 10%H_2-Ar atmosphere at 900 °C and 950 °C in order to evaluate its thermodynamic stability under reducing conditions. These materials seem to be stable until 900 °C, while at 950 °C a drift in the mass suggests a slow sample decomposition process, which was checked by XRD. A small peak corresponding to metallic Mo was detected in the XRD pattern of SMMMn powders thermally treated at 950 °C and cooled at room temperature under reducing atmosphere. Meanwhile, XRD studies for SMMO sample after being treated under the same atmosphere but at 1000 °C (not shown here) did not show any impurity peaks. Therefore, it can be concluded that transition metal doping at the Mo-site is a disadvantage to the phase stability under reducing conditions and high temperature. However, all SMMTM recover their initial mass after consecutive oxidation/reduction cycles at 800 °C

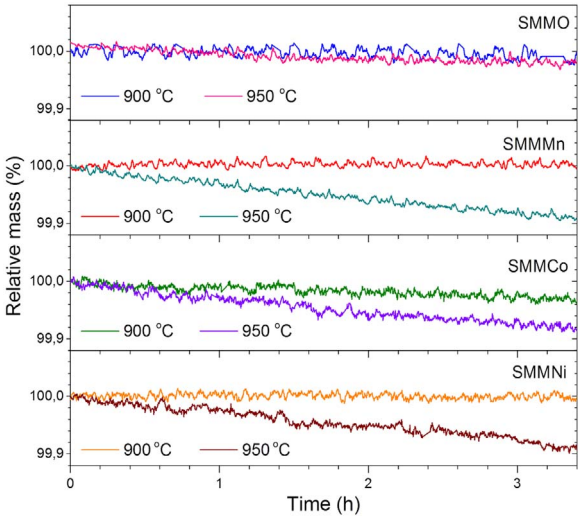

Fig. 3. Relative mass evolutions with time for SMMO and SMMTM compounds under reducing atmosphere (10%H_2-Ar) at 900 and 950 °C.

Fig. 4 shows the Arrhenius plot of the total electrical conductivity for SMMO and SMMTM within the temperature range 600–800 °C under 10%H_2-Ar and air. In both atmospheres, a linear dependence of the conductivity is observed, thus indicating a semiconductor-type behaviour for SMMO and SMMTM compounds with $\sigma = \left(\frac{A}{T}\right) exp\left(\frac{-E_a}{k_B T}\right)$ (where k_B is Boltzmann constant, A is a pre-exponential factor, and E_a is the activation energy including charge carrier formation energy and temperature activated mobility). Table 2 shows the conductivity values under equilibrium conditions obtained at 800 °C and the calculated activation energies (E_a).

The absolute values of conductivity obtained in 10%H_2-Ar atmosphere are more than three orders of magnitude higher than the values in air. This indicates that the electron conductivity is *n*-type in agreement with that proposed by Marrero-Lopez et al. [31]. The results for SMMO and SMMTM in 10%H_2-Ar at 800 °C showed that the partial substitution of Mo by Mn or Ni decreases slightly the electrical conductivity. Meanwhile, the highest electrical conductivity value under

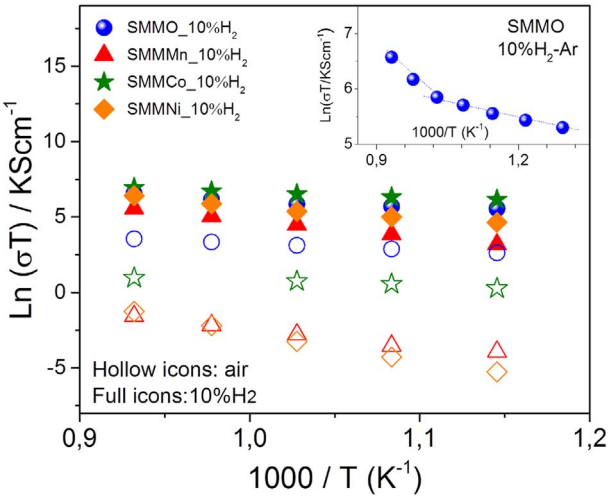

Fig. 4. Arrhenius plots of electrical conductivity for SMMTM (TM = Mn, Co and Ni) under reducing (full icons) and oxidising (hollow icons) atmospheres. Inset: $ln(\sigma T)$ vs 1000/Tplot for SMMO in 10%H_2-Ar.

reductive environment was obtained for SMMCo and SMMO compounds. Besides, TM-doping (TM = Mn, Co, and Ni) on Mo-site of the Sr_2MgMoO_6 has detrimental effects on the conductivity values of the compounds under air condition, i.e., the conductivity value decreases two order of magnitude.

The activation energies for SMMMn and SMMNi in 10%H_2-Ar (0.91 and 0.70 eV respectively) are higher than those of SMMCo and SMMO. The values for SMMO and SMMCo determined here are in agreement with those reported in literature for $Sr_2MgMoO_{6-\delta}$ under reducing atmosphere (0.19–0.3 eV approximately) [6,13,19,32]. Nevertheless, E_a values calculated here for SMMMn and SMMNi are close to those reported for $Sr_2MgMo_{0.8}Nb_{0.2}O_{6-\delta}$ [23]. The inset in Fig. 4 shows a detail of the $ln(\sigma T)$ vs 1000/T plot for $Sr_2MgMoO_{6-\delta}$ under diluted-H_2 atmosphere in the range of temperature between 500 and 800 °C, where two temperature regimes with activation energies 0.65 eV (700–800 °C) and ~ 0.18 eV (500–700 °C) can be observed. Similar results were reported by other authors for SMMO exposed to reducing atmospheres [21]. Some authors [31] attribute the reduction of the activation energy to the decrease in the hopping distance due to the increase of Mo^{5+} concentration. However, it was suggested that materials with mixed-conductivity (MIEC) generally present activation energies between 0.1 and 1.0 eV. Activation energies closer to 0.1 eV are thought to be an indicative of electron or electron-hole small polaron behaviour and those closer to 1.0 eV are thought to be cause by oxide ion mobility [33,34]. Thus, differences in the E_a values observed in these temperature-regimes could be attributed to different conduction mechanisms dominating the electrical conductivity. Based on these results, it can be inferred that the electrical conductivity dependence with temperature for SMMMn and SMMNi samples seems to be dominated by ionic transport. On the other hand, the electron transport is prevailing in SMMO and SMMCo compounds.

The electrical conductivity in $Sr_2MgMoO_{6-\delta}$-type compounds has proven to be strongly dependent on the synthesis conditions (oxidising and reducing atmosphere) and reduction degree of samples, which is determined by temperature and the time of the reduction treatment. Samples synthesised under reducing conditions have more oxygen vacancies than those synthesised in air [35]. The aforementioned statement can be observed in the wide range of conductivity values measured under reducing atmospheres published in literature [13,15,17,19,22,32,36].

Furthermore, the presence of small amounts of impurities such as $SrMoO_4$ [37] might positively impact on the electrical conductivity of SMMO/SMMTM; since in reducing conditions $SrMoO_4$ is reduced to $SrMoO_3$ [38,39] which presents high electronic conductivity. This could partially explain the high conductivity value (~ 9 S/cm) reported in literature for $Sr_2MgMoO_{6-\delta}$ [12,21,22]. As it was discussed above, SMMO [26] and SMMTM, synthesised in the present study, did not present $SrMoO_4$ as secondary phase (see Fig. 1).

Table 2 includes literature data in order to compare the effects of 10% doping in Sr_2MgMoO_6 with Ni and Co, either on Mg- [$Sr_2Mg_{0.9}Co_{0.1}MoO_{6-\delta}$ (SMCoM) and $Sr_2Mg_{0.9}Ni_{0.1}MoO_{6-\delta}$ (SMNiM)] or Mo-sites (SMMTM). In $Sr_2MgMoO_{6-\delta}$ both Sr and Mg-site are divalent; whereas the Mo-site can be multivalent (i.e +6, +5, +4, etc) and the partial replacement of Mg or Mo- sites by aliovalent elements must alter the concentration of oxygen vacancies and the electrical conductivity of these materials [12]. According to this, it is expected that the substitution of Mg^{2+} by other divalent metals does not affect the number of charge carriers (either electronic or ionic). In contrast to the above, the presence of divalent metals on Mo-site would increase the charge carriers, and thus the concentration of oxygen vacancies in SMMO compound. In this context, it was observed that the conductivity values in reducing atmosphere at 800 °C for SMNiM and SMMNi are similar. However, the activation energy for $Sr_2MgMo_{0.9}Ni_{0.1}O_{6-\delta}$ is higher than that of $Sr_2Mg_{0.9}Ni_{0.1}MoO_{6-\delta}$ [29], which is in agreement with a significant ionic contribution to the electrical conduction mechanisms. Besides, it was detected that even though E_a for SMMCo is slightly higher than the value reported for $Sr_2Mg_{0.9}Co_{0.1}MoO_{6-\delta}$ [20], the conductivity values at 800 °C are almost the same for both compounds. These results indicate that the substitution of Mo by Co or Ni in SMMCo and SMMNi compounds not only increases the oxygen vacancies concentration but they could also block the electron hopping through the Mo-site.

In regard to the electrochemical performance, an inadequate adhesion between the electrolyte and the anode as well as chemical reactions at the anode/electrolyte interface might create an insulating phase, increasing the electrode polarisation resistance [2,29]. Fig. 5a shows the formation of secondary phases such as $SrLaGa_3O_7$ and SrLa(GaO_4) when SMMO + LSGM mixture was treated at 1000 °C, while no trace of impurity phases was detected for SMMO + GDC at 1200 °C.

Table 2
Electrical conductivity at 800 °C, activation energy and area specific polarisation resistance (ASR) values for SMMO and SMMTM samples under diluted-H_2/air atmospheres. CS: Combustion-solution, NC: Nitrate-citrate route, FD: Freeze-drying precursor method. SMCoM: $Sr_2Mg_{0.9}Co_{0.1}MoO_{6-\delta}$ and SMNiM: $Sr_2Mg_{0.9}Ni_{0.1}MoO_{6-\delta}$.

		10%H_2-Ar_800 °C			Dry-air_ 800 °C		
Compound	**Synthesis**	**Ea (eV)**	**σ (S/cm)**	**ASR (× 10^{-2} Ω cm^2)**	**Ea (eV)**	**σ (S/cm)**	**ASR (Ω cm^2)**
SMMMn (this work)	CS	0.96 ± 0.06	0.25	1.1	0.98 ± 0.07	1.94 × 10^{-4}	3.9
SMMCo (this work)	CS	0.31 ± 0.03	0.80	4.9	0.27 ± 0.04	2.46 × 10^{-3}	2.5
SMCoM [20]	NC, 1450 °C -10 h air, then 5%H_2-24 h-800 °C	0.216	~ 0.84	126 (5%H_2)	–	–	–
SMMNi (this work)	CS	0.70 ± 0.07	0.57	10.6	1.62 ± 0.05	2.65 × 10^{-4}	3.3
SMNiM [29]	NC, 1450 °C -10 h air, then 5%H_2-24 h-800 °C	0.236	~ 0.65	150 (5%H_2)	–	–	–
SMMO (this work)	CS	0.176 and 0.65	0.67	1.2	0.38 ± 0.02	3.27 × 10^{-2}	12.2
SMMO [15]	FD, 1000 °C -5%H_2-24 h	0.19	0.8 (wet-H_2)	37 and 32 (wet-H_2) [31]	1.12	~ 3 × 10^{-3}	–
SMMO [13]	Sol-gel, 1200 °C -5%H_2-24 h	0.197	4.26 (5%H_2)	–	–	–	–

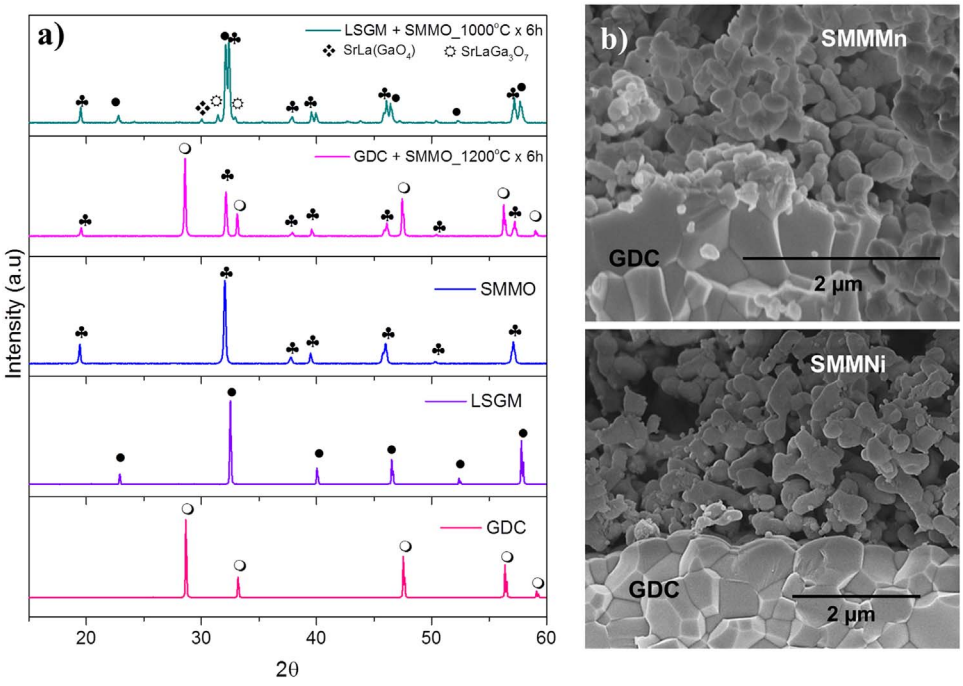

Fig. 5. a) XRD patterns of mixtures of Sr_2MgMoO_6 with LSGM and GDC powders, after thermal treatment at 1000 and 1200 °C respectively for 6 h **b)** SEM micrographs of the cross-section of the SMMMn/GDC and SMMNi/GDC interface for the symmetrical cells fired at 1000 °C during 3 h.

Fig. 5b shows the SEM micrographs corresponding to the SMMMn/GDC and SMMNi/GDC interfaces which indicates a seemingly good adhesion. Therefore, GDC was used as supporting electrolytes to evaluate the electrochemical response of SMMTM compounds.

Fig. 6 shows the representative EIS spectra for SMMO and SMMTM electrodes, with GDC as electrolyte, obtained under 10%H_2-Ar at 800 °C. The area specific polarisation resistance (ASR) values were calculated from the total polarisation resistance R_p and electrode surface S by: $ASR=\frac{R_pS}{2}$. The factor 2 is due to the symmetrical cell configuration.

The EIS spectra for symmetrical SMMO/GDC/SMMO and SMMTM/GDC/SMMTM cells in 10%H_2-Ar showed inductive effects and small resistance values for all samples. Similar behaviour was reported by other authors for SMMO samples measured under humidified-5%H_2-Ar [18]. For clarity in the figures, the high frequency intercept with real axis was subtracted.

The ASR approximate values for SMMO and SMMTM under 10%H_2-Ar at 800 °C are presented in Table 2. The obtained resistance values for SMMO and SMMTM (TM = Mn and Co) are around of 10^{-2} Ω cm^2. The partial substitution of Mo by Ni increases the ASR by one order of magnitude.

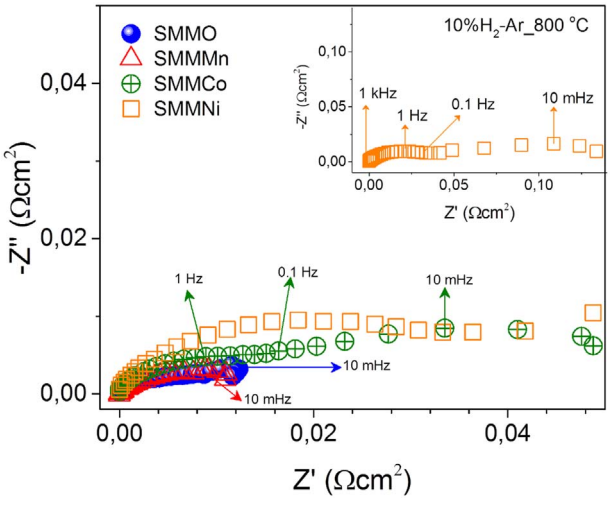

Fig. 6. Impedance spectra of symmetrical SMMO/GDC/SMMO and SMMTM/GDC/SMMTM cells measured under 10%H_2-Ar at 800 °C, inset: EIS spectrum for SMMNi.

EIS measurements show that Ni-doping on Mo-site of Sr_2MgMoO_6, is in detriment of the ASR. Nevertheless, ASR value for SMMNi, is lower than those obtained for $Sr_2Mg_{1-x}Ni_xMoO_{6-\delta}$ [29] where Ni is located on Mg-site. The ASR values for SMMO and SMMTM (TM = Mn and Co) are nearly two orders of magnitude lower than those of $Sr_2Mg_{1-x}Ni_xMoO_{6-\delta}$ [29], $Sr_2Mg_{1-x}Co_xMoO_{6-\delta}$ [20], and $Sr_2MgMo_{0.8}Nb_{0.2}O_{6-\delta}$ [23], which indicates the noteworthy effectiveness of doping on Mo-site. It is important to note that the maximum synthesis temperature for SMMO and SMMTM compounds here investigated was 1200 °C, whereas the compounds studied in the Ref. [20,23] were synthesised at temperature > 1300 °C, which increases the grain size and therefore the ASR values.

The difference between the ASR values reported in this work and those of literature could be associated to different synthesis conditions used by different authors, which have a strong impact on the microstructure of the materials. The total amount of particles at the electrode/electrolyte interface and its proper adhesion to the electrolyte are thus, parameters that affect the electrochemical response of the electrodes. The growth of grain size in the SMMTM powders (see Fig. 2) with increasing synthesis temperature may partially explain the difference observed between the ASR values in this work. In the Table 2 has been included synthesis methods (combustion-solution: CS, nitrate-citrate route: NC, freeze-drying precursor method: FD and sol-gel) and the temperatures of calcination used to obtain $Sr_2MgMoO_{6-\delta}$ compound and doped materials with 10% of Co or Ni either on Mg- or Mo-sites.

Fig. 7a shows the impedance spectra for symmetrical SMMO/GDC/SMMO and SMMTM/GDC/SMMTM cells under dry-air, by using LSM as current collector. Fig. 7b displays the Arrhenius plots of the ASR values for these symmetrical cells in the temperature range 600–800 °C. The approximate ASR values for LSM/SMMO/GDC/SMMO/LSM and LSM/SMMTM/GDC/SMMTM/LSM at 800 °C and E_a are summarised in Table 2.

EIS spectra (Fig. 7a) confirmed that partial substitution of Mo by transition metals (Mn, Co or Ni) in $Sr_2MgMoO_{6-\delta}$ compound decreases ASR values in air. However, these ASR values for

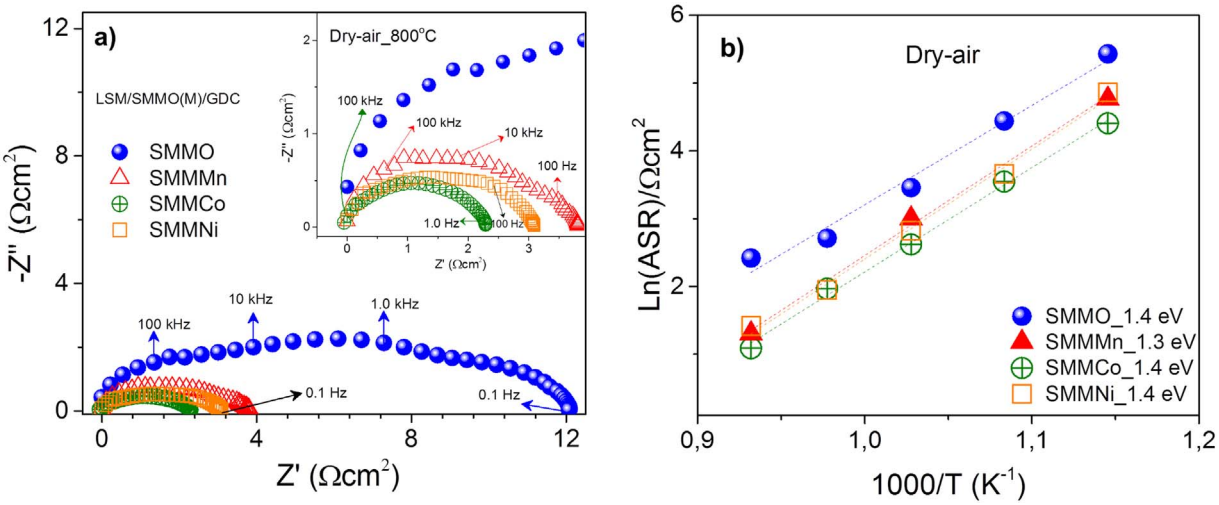

Fig. 7. Impedance spectra of symmetrical cells LSM/SMMO/GDC/SMMO/LSM and LSM/SMMTM/GDC/SMMTM/LSM measured in oxidising atmosphere. LSM acts as current collector **a)** Nyquist plot and **b)** Arrhenius plots of ASR values.

$Sr_2MgMo_{0.9}TM_{0.1}O_{6-\delta}$ in dry-air with LSM as current collector are higher than those reported for other cathode materials [40–42]. Nevertheless, the possibility of using these materials in a symmetrical SOFC cannot be discarded, especially taking into account their good anodic behaviour.

The ASR values are the result of interplay between microstructural (i.e. particle size and specific surface area) and intrinsic properties (electronic and ionic conductivity). Therefore, the effect of substitution at Mg- or Mo-site on the ASR values could be analysed considering that microstructure of SMMCo and $Sr_2Mg_{0.9}TM_{0.1}MoO_{6-\delta}$ ($Sr_2Mg_{0.9}Co_{0.1}MoO_{6-\delta}$ and $Sr_2Mg_{0.9}Ni_{0.1}MoO_{6-\delta}$) are similar (T of synthesis > 1200 °C) and coarser than those of SMMO, SMMMn and SMMNi reported here. Then, as particle size decreases the specific area increases, hence ASR decreases. On the other hand, intrinsic properties such as electronic and ionic conductivity impact on ASR values. In this context, the difference between ASR of $SrMg_{0.9}TM_{0.1}MoO_{6-\delta}$ and $Sr_2MgMo_{0.9}TM_{0.1}O_{6-\delta}$ compounds with TM = Co or Ni, could be explained based on the fact that electronic conductivity is higher in Co-containing than in Ni-containing compounds.

4. Conclusions

$Sr_2MgMo_{0.9}TM_{0.1}O_{6-\delta}$ (SMMTM; TM = Co, Mn, Ni) compounds were synthesised by the combustion method, in air, and they were characterised through XRD, TGA, conductivity and EIS measurements. Rietveld refinements of XRD data clearly suggest that TM-doping is incorporated on Mo-site of the Sr_2MgMoO_6 double perovskite. TGA experiments indicate thermodynamic stability at 900 °C under 10%H_2-Ar atmosphere for all samples. SMMTM samples exhibit *n*-type semiconductor behaviour with high conductivity values in reducing atmosphere. The activation energy of electrical conductivity takes values around ~ 0.3 eV for SMMCo and ~1 eV for SMMMn and SMMNi. $Sr_2MgMo_{0.9}Co_{0.1}O_{6-\delta}$ compound under reducing condition at 800 °C shows the maximum conductivity value (0.8 S/cm), this value, as also the activation energy value, is similar to that of Sr_2MgMoO_6. The substitution of Mo by Mn does not affect the ASR under reducing atmosphere (~ $10^{-2}\,\Omega\,cm^2$), while the anodic ASR increases for $Sr_2MgMo_{0.9}Co_{0.1}O_{6-\delta}$ and $Sr_2MgMo_{0.9}Ni_{0.1}O_{6-\delta}$ compounds (~ $10^{-1}\,\Omega\,cm^2$). However, this difference can be related to the increases of particle size. In air, the cathodic ASR is reduced by replacing Mo ions by Ni, Co and Mn ions. Finally, the 10% partial substitution of Mo by transition metals (Co and Ni) is more effective from the point of view of electrical and electrochemical properties than partial substitution of Mg by the same cations.

Acknowledgments

The authors kindly acknowledge the support of CNEA, CONICET – PIP 0565 and Agencia Nacional de Promoción Científica y Tecnológica (ANPCyT) to PICT 2013-01032. The English grammar revision of this manuscript by H. Troiani and M. Ferreiro is greatly acknowledged.

References

[1] H. Yokokawa, H. Tu, B. Iwanschitz, A. Mai, Fundamental mechanisms limiting solid oxide fuel cell durability, J. Power Sources 182 (2008) 400–412, http://dx.doi.org/10.1016/j.jpowsour.2008.02.016.
[2] J.B. Goodenough, Y.-H. Huang, Alternative anode materials for solid oxide fuel cells, J. Power Sources 173 (2007) 1–10, http://dx.doi.org/10.1016/j.jpowsour.2007.08.011.
[3] A. Orera, P.R. Slater, New chemical systems for solid oxide fuel cells, Chem. Mater. 22 (2010) 675–690, http://dx.doi.org/10.1021/cm902687z.
[4] M. Van Den Bossche, S. McIntosh, On the methane oxidation activity of $Sr_2(MgMo)_2O_{6-\delta}$: a potential anode material for direct hydrocarbon solid oxide fuel cells, J. Mater. Chem. 21 (2011) 7443–7451, http://dx.doi.org/10.1039/c1jm10523j.
[5] Y.-H. Huang, Double perovskites as anode, Science 312 (2006) 254–258, http://dx.doi.org/10.1126/science.1125877 (80-.).
[6] S. Vasala, M. Lehtimäki, S.C. Haw, J.M. Chen, R.S. Liu, H. Yamauchi, M. Karppinen, Isovalent and aliovalent substitution effects on redox chemistry of $Sr_2MgMoO_{6-\delta}$ SOFC-anode material, Solid State Ion. 181 (2010) 754–759, http://dx.doi.org/10.1016/j.ssi.2010.03.037.
[7] Y. Matsuda, M. Karppinen, Y. Yamazaki, H. Yamauchi, Oxygen-vacancy concentration in $A_2MgMoO_{6-\delta}$ double-perovskite oxides, J. Solid State Chem. 182 (2009) 1713–1716, http://dx.doi.org/10.1016/j.jssc.2009.04.016.
[8] J.C. Ruiz-Morales, J. Canales-Vázquez, C. Savaniu, D. Marrero-López, P. Núñez, W. Zhou, J.T.S. Irvine, A new anode for solid oxide fuel cells with enhanced OCV under methane operation, Phys. Chem. Chem. Phys. 9 (2007) 1821–1830, http://dx.doi.org/10.1039/b617266k.
[9] S. Tao, J.T.S. Irvine, Synthesis and characterization of $(La_{0.75}Sr_{0.25})Cr_{0.5}Mn_{0.5}O_{3-\delta}$, a redox-stable, efficient perovskite anode for SOFCs, J. Electrochem. Soc. 151 (2004) A252–A259, http://dx.doi.org/10.1149/1.1639161.
[10] M. Irshad, K. Siraj, R. Raza, A. Ali, P. Tiwari, B. Zhu, A. Rafique, A. Ali, M.K. Ullah, A. Usman, A brief description of high temperature solid oxide fuel cell's operation, materials, design, fabrication technologies and performance, Appl. Sci. 6 (75) (2016) 1–23, http://dx.doi.org/10.3390/app6030075 (2016).
[11] B. Shri Prakash, S. Senthil Kumar, S.T. Aruna, Properties and development of Ni/YSZ as an anode material in solid oxide fuel cell: a review, Renew. Sustain. Energy Rev. 36 (2014) 149–179, http://dx.doi.org/10.1016/j.rser.2014.04.043.
[12] A.K. Dorai, Y. Masuda, J.-H. Joo, S.-K. Woo, S.-D. Kim, Influence of Fe doping on the electrical properties of $Sr_2MgMoO_{6-\delta}$, Mater. Chem. Phys. 139 (2013) 360–363, http://dx.doi.org/10.1016/j.matchemphys.2013.02.039.
[13] Y.-H. Huang, R.I. Dass, J.C. Denyszyn, J.B. Goodenough, Synthesis and characterization of $Sr_2MgMoO_{6-\delta}$, J. Electrochem. Soc. 153 (2006) A1266, http://dx.doi.org/10.1149/1.2195882.
[14] C. Bernuy-Lopez, M. Allix, C.A. Bridges, J.B. Claridge, M.J. Rosseinsky, $Sr_2MgMoO_{6-\delta}$: structure, phase stability, and cation site order control of reduction, Chem. Mater. 19 (2007) 1035–1043 ⟨http://pubs.acs.org/doi/abs/10.1021/cm0624116⟩.
[15] D. Marrero-López, J. Peña-Martínez, J.C. Ruiz-Morales, D. Pérez-Coll, M.A.G.

Aranda, P. Núñez, Synthesis, Phase Stability and Electrical Conductivity of $Sr_2MgMoO_{6-\delta}$ Anode, n.d. <http://doi.org/10.1016/j.materresbull.2007.07.032>.
[16] D.W. Dees, T.D. Claar, D.C. Fee, Conductivity of porous Ni/ZrO_2-Y_2O_3 cermets, J. Electrochem. Soc. 134 (1987) 2141–2146.
[17] Y. Ji, Y.-H. Huang, J.-R. Ying, J.B. Goodenough, Electrochemical performance of La-doped $Sr_2MgMoO_{6-\delta}$ in natural gas, Electrochem. Commun. 9 (2007) 1881–1885, http://dx.doi.org/10.1016/j.elecom.2007.04.006.
[18] D. Marrero-López, J. Peña-Martínez, J.C. Ruiz-Morales, M.C. Martín-Sedeño, P. Núñez, High temperature phase transition in SOFC anodes based on $Sr_2MgMoO_{6-\delta}$, J. Solid State Chem. 182 (2009) 1027–1034, http://dx.doi.org/10.1016/j.jssc.2009.01.018.
[19] Z. Xie, H. Zhao, T. Chen, X. Zhou, Z. Du, Synthesis and electrical properties of Al-doped $Sr_2MgMoO_{6-\delta}$ as an anode material for solid oxide fuel cells, Int. J. Hydrog. Energy 36 (2011) 7257–7264, http://dx.doi.org/10.1016/j.ijhydene.2011.03.075.
[20] Z. Xie, H. Zhao, Z. Du, T. Chen, N. Chen, X. Liu, S.J. Skinner, Effects of Co doping on the electrochemical performance of double perovskite oxide $Sr_2MgMoO_{6-\delta}$ as an anode material for solid oxide fuel cells, J. Phys. Chem. C 116 (2012) 9734–9743.
[21] L. Kong, B. Liu, J. Zhao, Y. Gu, Y. Zhang, Synthesis of nano-crystalline $Sr_2MgMoO_{6-\delta}$ anode material by a sol–gel thermolysis method, J. Power Sources 188 (2009) 114–117, http://dx.doi.org/10.1016/j.jpowsour.2008.11.134.
[22] F.Y. Wang, G. Bin Zhong, S. Luo, L. Xia, L.H. Fang, X. Song, X. Hao, G. Yan, Porous $Sr_2MgMo_{1-x}V_xO_{6-\delta}$ ceramics as anode materials for SOFCs using biogas fuel, Catal. Commun. 67 (2015) 108–111, http://dx.doi.org/10.1016/j.catcom.2015.04.019.
[23] M.J. Escudero, I. Gómez de Parada, A. Fuerte, L. Daza, Study of $Sr_2Mg(Mo_{0.8}Nb_{0.2})O_{6-\delta}$ as anode material for solid oxide fuel cells using hydrocarbons as fuel, J. Power Sources 243 (2013) 654–660, http://dx.doi.org/10.1016/j.jpowsour.2013.05.198.
[24] K.C. Patil, S.T. Aruna, T. Mimani, Combustion synthesis: an update, Curr. Opin. Solid State Mater. Sci. 6 (2002) 507–512, http://dx.doi.org/10.1016/S1359-0286(02)00123-7.
[25] C.M. Chanquía, A. Montenegro-Hernández, H.E. Troiani, A. Caneiro, A bottom-up building process of nanostructured $La_{0.75}Sr_{0.25}Cr_{0.5}Mn_{0.5}O_{3-\delta}$ electrodes for symmetrical-solid oxide fuel cell: synthesis, characterization and electrocatalytic testing, J. Power Sources 245 (2014) 377–388, http://dx.doi.org/10.1016/j.jpowsour.2013.06.124.
[26] P.K. Dager, C.M. Chanquía, L. Mogni, A. Caneiro, Synthesis of pure-phase Sr_2MgMoO_6 nanostructured powder by the combustion method, Mater. Lett. 141 (2015) 248–251, http://dx.doi.org/10.1016/j.matlet.2014.11.037.
[27] J. Rodríguez-Carvajal, Recent advances in magnetic structure determination by neutron powder diffraction, Phys. B Condens. Matter 192 (1993) 55–69, http://dx.doi.org/10.1016/0921-4526(93)90108-I.
[28] A. Caneiro, Adaptation of an electrochemical system for measurement and regulation of oxygen partial pressure to a symmetrical thermogravimetric analysis system developed using a Cahn 1000 electrobalance, Rev. Sci. Instrum. 53 (1982) 1072–1075, http://dx.doi.org/10.1063/1.1137090.
[29] Z. Xie, H. Zhao, Z. Du, T. Chen, N. Chen, Electrical chemical and electrochemical properties of double perovskite oxides $Sr_2Mg_{1-x}Ni_xMoO_{6-\delta}$ as anode materials for solid fuel cells, J. Phys. Chem. C 118 (2014) 18853–18860.
[30] F. Sher, A. Venimadhav, M.G. Blamire, B. Dabrowski, S. Kolesnik, J.P. Attfield, Structural, magnetic and transport properties of $Sr_2Fe_{1-x}Mg_xMoO_6$ double perovskites, Solid State Sci. 7 (2005) 912–919, http://dx.doi.org/10.1016/j.solidstatesciences.2005.03.002.
[31] D. Marrero-López, J. Peña-Martínez, J.C. Ruiz-Morales, M. Gabás, P. Núñez, M.A.G. Aranda, J.R. Ramos-Barrado, Redox behaviour, chemical compatibility and electrochemical performance of $Sr_2MgMoO_{6-\delta}$ as SOFC anode, Solid State Ion. 180 (2010) 1672–1682, http://dx.doi.org/10.1016/j.ssi.2009.11.005.
[32] L. Zhang, T. He, Performance of double-perovskite $Sr_{2-x}Sm_xMgMoO_{6-\delta}$ as solid-oxide fuel-cell anodes, J. Power Sources 196 (2011) 8352–8359, http://dx.doi.org/10.1016/j.jpowsour.2011.06.064.
[33] X. Dong, P. Gardner, T.L. Reitz, F. Chen, P. Directorate, A. Force, perovskite materials for use as sulfur tolerant anodes in SOFCS, in: S.M.T. Ohji (Eds.), Advances in Solid Oxide Fuel Cells VI: Ceramic Engineering and Science Proc., New Jersey, 2010: pp. 31–41.
[34] T.G. Howell, C.P. Kuhnell, T.L. Reitz, A.M. Sukeshini, R.N. Singh, A_2MgMoO_6 (A = Sr, Ba) for use as sulfur tolerant anodes, J. Power Sources 231 (2013) 279–284, http://dx.doi.org/10.1016/j.jpowsour.2013.01.004.
[35] S. Vasala, Properties and applications of $A_2B'B''O_6$ perovskites: from fuel cells to quasi-low-dimensional magnetism, Sch. Chem. Technol. (2014) http://urn.fi/URN:ISBN:978-952-60-5937-2.
[36] C. Graves, B.R. Sudireddy, M. Mogensen, Molybdate based ceramic negative-electrode materials for solid oxide cells, ECS Trans. 28 (11) (2010) 173–192, http://dx.doi.org/10.1149/1.3495841.
[37] S. Vasala, H. Yamauchi, M. Karppinen, Role of $SrMoO_4$ in Sr_2MgMoO_6 synthesis, J. Solid State Chem. 184 (2011) 1312–1317, http://dx.doi.org/10.1016/j.jssc.2011.03.045.
[38] I. Nagai, N. Shirakawa, S.I. Ikeda, R. Iwasaki, H. Nishimura, M. Kosaka, Highest conductivity oxide $SrMoO_3$ grown by a floating-zone method under ultralow oxygen partial pressure, Appl. Phys. Lett. 87 (2005) 1–4, http://dx.doi.org/10.1063/1.1992671.
[39] T. Maekawa, K. Kurosaki, H. Muta, M. Uno, S. Yamanaka, Thermal and electrical properties of perovskite-type strontium molybdate, J. Alloy. Compd. 390 (2005) 314–317, http://dx.doi.org/10.1016/j.jallcom.2004.08.038.
[40] L.V. Mogni, K. Yakal, C. Chanquía, Z. Gao, H. Wang, A. Caneiro, S. Barnett, Study of electrode performance for nanosized $La_{0.4}Sr_{0.6}Co_{0.8}Fe_{0.2}O_{3-\delta}$ IT-SOFC cathode, ECS Trans. 66 (2015) 169–176.
[41] J. Piao, K. Sun, N. Zhang, X. Chen, S. Xu, D. Zhou, Preparation and characterization of $Pr_{1-x}Sr_xFeO_3$ cathode material for intermediate temperature solid oxide fuel cells, J. Power Sources 172 (2007) 633–640, http://dx.doi.org/10.1016/j.jpowsour.2007.05.023.
[42] Q. Liu, X. Dong, G. Xiao, F. Zhao, F. Chen, A novel electrode material for symmetrical SOFCs, Adv. Mater. 22 (2010) 5478–5482, http://dx.doi.org/10.1002/adma.201001044.